An Optimal Multiedge Detector for SAR Image Segmentation

Roger Fjørtoft, Armand Lopès, Philippe Marthon, *Associate Member, IEEE*, and Eliane Cubero-Castan

Abstract— **Edge detection is a fundamental issue in image analysis. Due to the presence of speckle, which can be modeled as a strong, multiplicative noise, edge detection in synthetic aperture radar (SAR) images is extremely difficult, and edge detectors developed for optical images are inefficient. Several robust operators have been developed for the detection of isolated step edges in speckled images. We here propose a new step edge detector for SAR images, which is optimal in the minimum mean square error (MSSE) sense under a stochastic multiedge model. It computes a normalized ratio of exponentially weighted averages (ROEWA) on opposite sides of the central pixel. This is done in the horizontal and vertical direction, and the magnitude of the two components yields an edge strength map. Thresholding of the edge strength map by a modified version of the watershed algorithm and region merging to eliminate false edges complete an efficient segmentation scheme. Experimental results obtained from simulated SAR images as well as ERS-1 data are presented.**

Index Terms— **Edge detection, multiedge model, region merging, segmentation, speckle, synthetic aperture radar (SAR), watershed algorithm.**

I. Introduction

SEGMENTATION is the decomposition of an image in regions, i.e., spatially connected, nonoverlapping sets of pixels sharing a certain property. A region may for example be characterized by constant reflectivity or texture. Region-based segmentation schemes, such as histogram thresholding and split-and-merge algorithms, try to define regions directly by their content, whereas edge-based methods try to identify the transitions between different regions.

In images with no texture, an edge can be defined as an abrupt change in reflectivity. In the case of optical images, an edge is usually defined as a local maximum of the gradient magnitude in the gradient direction, or equivalently, as a zero-crossing of the second derivative in the direction of the gradient. Smoothing is necessary prior to derivation, as differential operators are sensitive to noise. The smoothing and differentiation operations are merged and implemented by two-dimensional (2-D) filters. Gradient-based edge detection basically consists in calculating the *difference* of the local radiometric means on opposite sides of the central pixel. This is done for every pixel position in the vertical and horizontal direction, and the magnitude of the components is computed. Finally, local maxima of the gradient magnitude image are extracted.

Owing to the multiplicative nature of speckle, edge detectors based on the difference of average pixel values detect more false edges in areas of high reflectivity than in areas of low reflectivity in synthetic aperture radar (SAR) images [1]. Certainly, other measures than the difference can be used to identify abrupt transitions. Several edge detectors with constant false alarm rates (CFAR's) have been developed specifically for SAR images, e.g., based on a ratio of averages [1], [2] or a likelihood ratio [3], [4]. However, these operators use the arithmetic mean for the estimation of local mean values, which is optimal only in the monoedge case. Segmentation schemes based on region growing [5], [6], histogram thresholding [7], and simulated annealing [8] have also been proposed for SAR images.

In this article we concentrate on the spatial aspect of edge detection, based on a multiedge model. We incorporate the specific properties of SAR images and develop a linear minimum mean square error (MMSE) filter for the estimation of local mean values. In this way we obtain a new edge detector with improved noise suppression and edge detection properties. Section II explains the principle of monoedge detection in SAR imagery. In section III we develop an optimal multiedge detector and propose a thresholding method which extracts closed, skeleton boundaries. The use of region merging to eliminate false edges is also described. Experimental results obtained from simulated SAR images and ERS-1 data are presented in section IV. We discuss theoretical aspects and experimental results in section V, and end with some concluding remarks in section VI.

II. Monoedge detection in SAR images

Speckle is a deterministic effect common to all imaging systems relying on coherent illumination. It is due to the constructive and destructive interference of the responses of the different elementary scatterers of a resolution cell. In the measured intensity image I, speckle is well modeled as a multiplicative random noise n, which is independent

Manuscript received December 30, 1996; revised August 13, 1997. This work was supported by the French Space Agency (CNES) under Contract 833/CNES/94/1022/00.

R. Fjørtoft and A. Lopès are with the Centre d'Etudes Spatiales de la Biosphère (CESBIO), UMR 5639 CNES/CNRS/UPS, 31401 Toulouse, France (e-mail: Roger.Fjortoft@cesbio.cnes.fr; Armand.Lopes@cesbio.cnes.fr).

P. Marthon is with the Laboratoire d'Informatique et de Mathématiques Appliquées (LIMA), Ecole Nationale Supérieure d'Electrotechnique, d'Electronique, d'Informatique et d'Hydraulique de Toulouse (ENSEEIHT), Institut de Recherche en Informatique de Toulouse (IRIT), UMR 5505 UPS/INP/CNRS, 31071 Toulouse, France (e-mail: Philippe.Marthon@enseeiht.fr).

E. Cubero-Castan is with the French Space Agency (CNES), DGA/T/SH/QTIS, 31401 Toulouse, France (e-mail: Eliane.Cubero-Castan@cnes.fr).

Publisher Item Identifier S 0196-2892(98)01195-4.

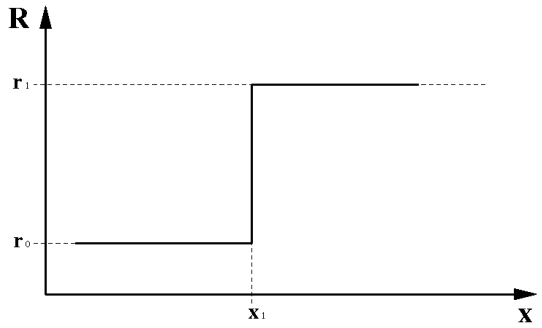

Fig. 1. One-dimensional monoedge model.

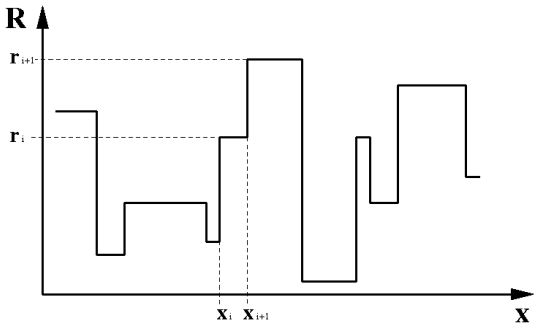

Fig. 2. One-dimensional multiedge model.

of the radar reflectivity R [9]

$$I(x) = R(x) \cdot n(x). \tag{1}$$

The transfer function of the SAR system is designed to vary as little as possible over the bandwidth of interest. It is known to have negligible influence on the spectrum of the ideal image, but to limit the bandwidth of the noise spectrum. This effect is here incorporated in the term n. Fully developed speckle is Gamma distributed with mean value $\mu_n = 1$ and variance $\sigma_n^2 = 1/L$, where L is the equivalent number of independent looks (ENIL) of the image [9].

Several CFAR edge detectors have been developed for SAR images based on the monoedge model, which supposes that only one step edge is present in the analyzing window (Fig. 1). For example, Touzi *et al.* showed that edge detectors based on the Ratio Of Averages (ROA) have CFAR, because the standard deviation σ_I is proportional to the mean intensity μ_I [1]. The ratio is normalized to lie between zero and one

$$r_{\min} = \min\left\{\frac{\hat{\mu}_1}{\hat{\mu}_2}, \frac{\hat{\mu}_2}{\hat{\mu}_1}\right\} \tag{2}$$

where $\hat{\mu}_1$ and $\hat{\mu}_2$ are the arithmetic mean intensities of the two halves of a window of fixed size. The normalized ratio is calculated in four (or more) directions, by splitting the analyzing window along the horizontal, vertical and diagonal axes. The minimum of the four values thus obtained is finally compared to an edge detection threshold, which is set according to the accepted probability of false alarm (PFA), i.e., the probability of detecting an edge in a zone of constant reflectivity.

The principle of the likelihood ratio (LR) detector is to estimate the ratio of the probability that the analyzing window covers two regions separated by a given axis to the probability that the entire window belongs to one single region. Transforming the LR for edge detection in SAR images into a log-likelihood difference yields [4]

$$\ell_{\text{edge}} = \nu\left(-N_1 \log \hat{\mu}_1 - N_2 \log \hat{\mu}_2 + N_0 \log \hat{\mu}_0\right) \tag{3}$$

where ν is the order parameter of the Gamma distribution of the SAR image, N_1, N_2, $\hat{\mu}_1$, and $\hat{\mu}_2$ are the number of pixels and the arithmetic mean values of the two half windows, and N_0 and $\hat{\mu}_0$ are the corresponding parameters for the entire window. Oliver *et al.* recently showed that the ROA operator coincides with the LR operator if only the averages are estimated on equally sized halves of the sliding window [4].

The unbiased maximum likelihood (ML) estimator of the mean value of a Gamma distributed *stationary* process, is the arithmetic mean [4]. The ROA and LR operators both use this estimator. It is optimal under the monoedge model, i.e., as long as the width of each half window does not exceed the minimum distance between significant edges. In SAR images the signal to noise ratio is very low, typically 0 dB for single-look images. To sufficiently reduce the influence of the speckle, an important number of pixels must be averaged in each half window. So there is a conflict between strong speckle reduction and high spatial resolution, and the chosen window size constitutes a compromise between these two requirements. This illustrates the limitations of the monoedge model.

III. Multiedge detection in SAR images

For most scene types, the large windows that we use to detect edges in SAR images are likely to contain several edges simultaneously. In fact, we need to estimate the *local mean values* $\{\hat{\mu}_{r_i}\}$ of a signal which undergoes abrupt transitions with random intervals. The monoedge hypothesis is generally not verified, and the arithmetic mean is no longer optimal. Estimators with nonuniform weighting should therefore be considered. The filter coefficients decide the weighting of the pixels as a function of the distance to the central pixel. For our application, they should optimize the tradeoff between noise suppression and spatial resolution, based on *a priori* knowledge of image and noise statistics.

A. Multiedge model

We restrict ourselves to a separable image model. In the horizontal as well as in the vertical direction we suppose that the reflectivity image (ideal image) R is a stationary random process composed by piecewise constant segments of reflectivity $\{r_i\}$, with mean value μ_r and standard deviation σ_r. The localization of the reflectivity jumps $\{x_i\}$ follows a Poisson distribution with parameter λ corresponding to the mean jump frequency, i.e., the probability of k jumps in the interval Δx is given by

$$p_k(\Delta x) = \frac{(\lambda \Delta x)^k}{k!} e^{-\lambda \Delta x}.$$

The reflectivities $\{r_i\}$ and the jump localizations $\{x_i\}$ are supposed to be independent. Hence $\mu_R = \mu_r$ and $\sigma_R^2 = \sigma_r^2$. Fig. 2 illustrates the multiedge model in the one-dimensional (1-D) case. Although it is idealized, this model

is a good approximation for important scene types, such as agricultural fields.

It can easily be shown that the autocovariance function of the reflectivity is [10]:

$$C_{RR}(\Delta x) = \sigma_r^2 e^{-\lambda|\Delta x|}.$$

The ideal image is thus a separable first-order Markov process with parameter λ. The power spectral density, which we here define as the Fourier transform of the autocovariance function, is then

$$S_{RR}(\omega) = \frac{2\lambda\sigma_r^2}{\lambda^2 + \omega^2}. \quad (4)$$

B. Linear MMSE filter

Let us now develop the linear MSSE filter for the estimation of the local mean under the stochastic multiedge model and the multiplicative noise model. It should not be confused with an adaptive speckle filter [11], which restores the reflectivity of a pixel based on the local statistics. The MMSE filter will be split along the vertical and horizontal axes, and the weighted means estimated in the different half windows will be used for edge detection. To facilitate the implementation, we suppose the filter to have separable impulse response $f_{2\text{-D}}(x,y) = f(x)f(y)$ and first consider the one-dimensional case. The best unbiased linear estimator of the reflectivity is of the form [12]

$$\hat{R}(x) = \mu_R + f(x) * (I(x) - \mu_I). \quad (5)$$

Minimizing the mean square error $E\left[|R(x) - \hat{R}(x)|^2\right]$ yields the transfer function [12]

$$F(\omega) = \frac{\mu_n S_{RR}(\omega)}{S_{RR}(\omega) * S_{nn}(\omega) + \mu_R^2 S_{nn}(\omega) + \mu_n^2 S_{RR}(\omega)}. \quad (6)$$

The autocovariance function of the speckle decreases very rapidly [9]. As an approximation, n will be considered as white noise here

$$C_{nn}(\Delta x) = \sigma_n^2 \delta(\Delta x)$$

$$S_{nn}(\omega) = \sigma_n^2 = 1/L$$

By substituting the power spectral densities and mean values into (6) and taking the inverse Fourier transform we obtain the optimal impulse response

$$f(x) = Ce^{-\alpha|x|}$$

where

$$\alpha^2 = \frac{2L\lambda}{1 + (\mu_R/\sigma_R)^2} + \lambda^2 \quad (7)$$

and C is a normalizing constant. From the multiplicative noise model (1) we have $\mu_R = \mu_I$ and

$$\sigma_R^2 = \frac{L\sigma_I^2 - \mu_I^2}{L+1}$$

which can be estimated from the speckled image. The average region width $1/\lambda$ can be evaluated visually, or we can estimate λ from the spectrum of a speckle-reduced image (4) obtained by adaptive filtering [11].

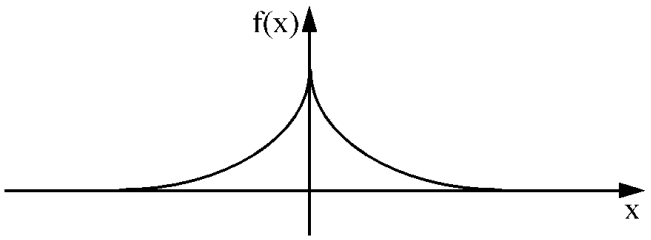

Fig. 3. Impulse response of the infinite symmetric exponential filter (ISEF).

We normalize f with respect to the mean value, i.e., $C = \alpha/2$, to obtain an unbiased estimator. With this normalization $f(x) * \mu_I = \mu_I$ and (5) simplifies to

$$\hat{R}(x) = f(x) * I(x).$$

We can thus apply the filter directly to the measured intensity image I.

The impulse response of $f(x)$ is shown in Fig. 3. As we see, the filter is of infinite extent, which for the two-dimensional filter $f_{2\text{-D}}(x,y) = f(x)f(y)$ means that the analyzing window centered on the pixel to be filtered covers the entire image. The weight of the surrounding pixels decreases exponentially with distance. The further a pixel is from the center, the more likely it is to belong to another region, and the less influence it has on the estimated local mean. We note that $f_{2\text{-D}}$ is not strictly isotropic.

The filter f is known as the infinite symmetric exponential filter (ISEF). The ISEF is the basis of the edge detector of Shen and Castan [13], which computes the difference of the exponentially weighted means in each half window. This is an optimal multiedge detector for images degraded by additive white noise. It is claimed to have better edge localization precision than other edge detectors proposed for optical images [13]. We have now shown that the same type of smoothing filter is optimal in the case of multiplicative noise. However, as explained in section I, edge detectors based on the difference of averages are not suited for SAR images.

We also note the analogy between the ISEF and the Frost speckle filter [11]. Frost *et al.* assumed the *local* variations, within stationary regions of the image, to be a first order Markov process and developed an adaptive restoration filter where local statistics control the slope of the exponential weighting function. We use the first order Markov process as a *global* image model for the optimization of a nonadaptive filter.

In the discrete case, f can be implemented very efficiently by a pair of recursive filters [13], [14]. We define two discrete filters, $f_1(n)$ and $f_2(n)$, realizing the normalized causal and anti-causal part of $f(n)$, respectively

$$f_1(n) = a \cdot b^n u(n), \quad (8)$$

$$f_2(n) = a \cdot b^{-n} u(-n), \quad (9)$$

where $0 < b = e^{-\alpha} < 1$, $a = 1 - b$, and $u(n)$ is the discrete Heaviside function. The smoothing function can now be rewritten as

$$f(n) = c \cdot b^{|n|} \equiv \frac{1}{1+b} f_1(n) + \frac{b}{1+b} f_2(n-1)$$

where $c = (1-b)(1+b)$.

By taking the z-transform of (8) and (9) we obtain

$$\begin{aligned} F_1(z) &= \frac{a}{1-bz^{-1}} \\ F_2(z) &= \frac{a}{1-bz} \end{aligned}$$

In terms of the spatial index n, convolution with $f_1(n)$ and $f_2(n)$ corresponds to the following simple recursions

$$\begin{aligned} s_1(n) &= a\,e_1(n) \\ &\quad + b\,s_1(n-1) \qquad n = 1,\ldots,N \qquad (10) \\ s_2(n) &= a\,e_2(n) \\ &\quad + b\,s_2(n+1) \qquad n = N,\ldots,1. \qquad (11) \end{aligned}$$

Here $e_1(n)$ and $e_2(n)$ are the inputs, and $s_1(n)$ and $s_2(n)$ are the outputs of f_1 and f_2, respectively. To minimize the number of multiplications, we may rewrite (10) and (11) as

$$\begin{aligned} s_1(n) &= a\,(e_1(n) - s_1(n-1)) \\ &\quad + s_1(n-1) \qquad n = 1,\ldots,N \\ s_2(n) &= a\,(e_2(n) - s_2(n+1)) \\ &\quad + s_2(n+1) \qquad n = N,\ldots,1. \end{aligned}$$

The computational cost for f_1 and for f_2 is thus one multiplication per pixel. Due to the normalizing factors, f necessitates four multiplications per pixel.

C. The ROEWA operator

Based on the linear MMSE filters described above, we propose a new ratio-based edge detector: the *ratio of exponentially weighted averages* (ROEWA) operator. The exponentially weighted averages $\hat{\mu}_1$ and $\hat{\mu}_2$ are normalized to be unbiased, and we show in the Appendix that their variance is proportional to the variance of the raw image. The standard deviation remains proportional to the mean value, so the ROEWA operator has CFAR [1]. As opposed to Touzi *et al.*, (2), we normalize the ratio to be superior to one

$$r_{\max} = \max\left\{\frac{\hat{\mu}_1}{\hat{\mu}_2}, \frac{\hat{\mu}_2}{\hat{\mu}_1}\right\}. \qquad (12)$$

The two approaches are of course equivalent. Our choice is motivated by the particular algorithm that we use in the edge extraction step.

To compute the horizontal edge strength component, the image $I(x,y)$ is first smoothed column by column using the one-dimensional smoothing filter f. Next, the causal and anti-causal filters f_1 and f_2 are employed line by line on the result of the smoothing operation to obtain $\hat{\mu}_1(x)$ and $\hat{\mu}_2(x)$

$$\begin{aligned} \hat{\mu}_{X1}(x,y) &= f_1(x) * (f(y) \star I(x,y)) \\ \hat{\mu}_{X2}(x,y) &= f_2(x) * (f(y) \star I(x,y)). \end{aligned}$$

Here $*$ denotes convolution in the horizontal direction and $\star$ denotes convolution in the vertical direction. The normalized ratio $r_{X\,\max}(x,y)$ is found by substituting $\hat{\mu}_{X1}(x-1,y)$ and $\hat{\mu}_{X2}(x+1,y)$ into (12). The vertical edge strength component is obtained in the same manner, except that the directions are interchanged

$$\begin{aligned} \hat{\mu}_{Y1}(x,y) &= f_1(y) \star (f(x) * I(x,y)) \\ \hat{\mu}_{Y2}(x,y) &= f_2(y) \star (f(x) * I(x,y)). \end{aligned}$$

Finally, with analogy to gradient based edge detectors for optical images, we take the magnitude of the two components

$$|r_{\text{2-D}\,\max}(x,y)| = \sqrt{r^2_{X\,\max}(x,y) + r^2_{Y\,\max}(x,y)}.$$

In the edge strength map thus obtained, a high pixel value indicates the presence of an edge. For each pixel this implies a total of 14 multiplications, an average of 3 divisions, and 1 square root operation.

D. Edge extraction

By thresholding the edge strength map we obtain pixels which, with a certain PFA, belong to edges. If the threshold is set too high, we miss important edges, and if it is set too low, we detect a lot of false edges. Plain thresholding will in general produce several pixel wide, isolated edge segments. The edges can be thinned to unity width e.g., using morphological closing [1]. The problem of forming closed boundaries from spatially separated edge segments is quite complicated. If the edges are not closed, they do not define a segmentation of the image.

The *watershed algorithm* [15] is a simple and efficient edge detection method which gives closed, skeleton boundaries. The edge strength map is considered as a surface and the algorithm detects local maxima by immersion simulation. In its original form, the watershed algorithm retains all of the local maxima of the edge strength map, which separate different basins. It unfortunately tends to produce massively over-segmented images. We have chosen to introduce an edge detection threshold in the algorithm [16]. Only edge strength magnitudes over the chosen threshold are considered. Local maxima with lower magnitudes are supposed to be due to noise. With this modification, the algorithm detects, thins and closes significant edges in one operation. The modified watershed algorithm is illustrated in Fig. 4.

We do not have any analytical expression for the distribution of the exponentially weighted means. When the slope of the exponential function is moderate, however, we may suppose a Gaussian distribution according to the central limit theorem. The variance of the distribution as a function of the variance of the raw image, the speckle correlation and the filter parameter b is given in the Appendix. The relation between detection threshold and PFA can be established theoretically for the ROEWA operator based on the Gaussian hypothesis. In fact, as the Gamma distribution fits a Gaussian distribution very closely when the ENIL is a few tenths or higher, the PFA computed for the ROA operator [1] can also be used for the ROEWA for typical values of b. The ENIL of the exponentially weighted mean is equal to the ENIL of the raw image multiplied by the equivalent number of independent pixels in the half window, which is given in the Appendix. The PFA applies to the vertical or horizontal edge strength component, but only as an approximation to their magnitude. Moreover,

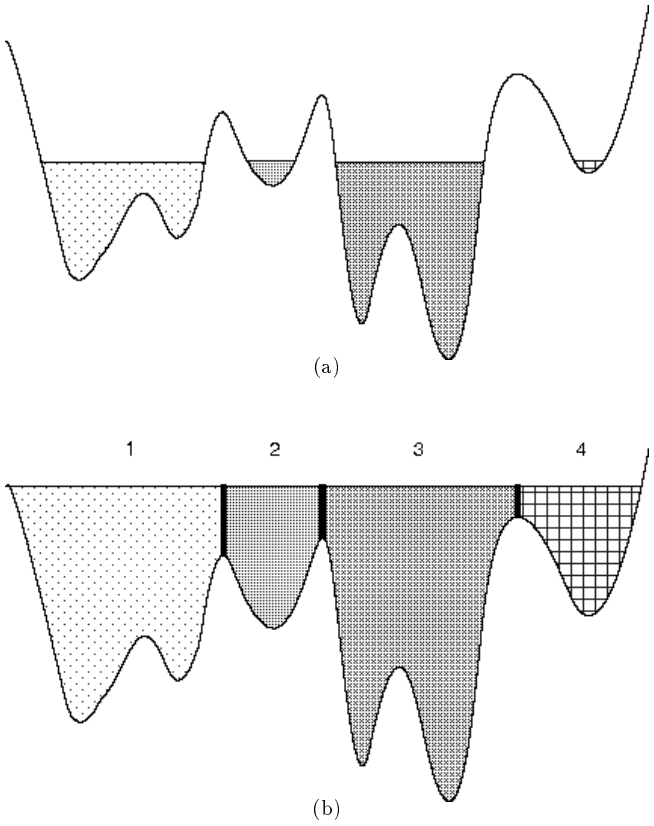

Fig. 4. (a) Initial state of the modified watershed algorithm shown on a cross-section of an edge strength map. (b) Skeleton boundaries detected after complete immersion.

watershed thresholding reduces the PFA compared to plain thresholding, as also false edges are thinned to unity width. The effect of this nonlinear operation is difficult to quantify. With our approach, the theoretical PFA for a given threshold can therefore only serve as a rough indication.

A particularity of watershed thresholding is that the whole edge is eroded if the edge strength magnitude of one single edge pixel is below the detection threshold. The threshold must consequently be set relatively low for the algorithm to form meaningful boundaries, but then we are bound to detect numerous false edges as well.

E. Post-processing

Spurious edges can be eliminated by merging adjacent regions whose reflectivities are not significantly different. Several merging criteria have been proposed, including the Student's t-test [6] and the unequal variance Student's t-test [14]. The LR of Oliver *et al.* [4] can also be used to decide whether or not two regions should be merged, and again constitutes an optimal criterion. In fact, $\ell_{\text{merge}} = -\ell_{\text{edge}}$ (3)

$$\ell_{\text{merge}} = \nu \left(N_1 \log \hat{\mu}_1 + N_2 \log \hat{\mu}_2 - N_0 \log \hat{\mu}_0 \right). \qquad (13)$$

Thus $\ell_{\text{merge}} \leq 0$, and a value close to zero suggests that the two regions together form a Gamma-homogeneous region. It should be noted, however, that we in many applications seek a thematic segmentation, so that weak textures within the regions can be accepted. In practice, negative thresholds are used. The more irregularities we accept within the regions, the further the threshold can be from zero. Again, the threshold can be related to the PFA [4].

Geometrical considerations, such as region size [14] and edge regularity [6], may also be taken into account in the merging process, based on *a priori* knowledge about the size and shape of the regions. The order in which the regions are merged has a strong influence on the final result. Finding the globally optimal merging order requires much time-consuming sorting. The *iterative pairwise mutually best merge criterion* [17] is a locally optimal approach which is much quicker. First all regions are compared with their neighbors in terms of the merging criterion, and the results are stored in a dynamic array. The array is then traversed sequentially, and a region $\mathcal{A}$ is merged with an adjacent region $\mathcal{B}$ if and only if $\mathcal{B}$ is the closest neighbor of $\mathcal{A}$ according to the merging criterion, and if $\mathcal{A}$ is also the closest neighbor of $\mathcal{B}$. When two regions are merged, the local statistics of the resulting region must be updated and the comparison with all its neighbors must be redone before continuing. The array is traversed repeatedly until no adjacent regions satisfy the merging criterion.

IV. Experimental results

The novelty of our detector is that it relies on weighted means rather than on the arithmetic means used by other CFAR detectors. To study the influence of the nonuniform weighting, we compare the ROEWA operator with the ROA operator. For both detectors the normalized ratio r_{max} is computed vertically and horizontally, and the magnitude of the two components constitutes the edge strength map. We use the modified watershed algorithm for thresholding, because it directly yields skeleton boundaries, localized on local maxima of the edge strength map. This property facilitates the subsequent tests.

A quantitative comparison of edge detectors can only be effectuated on simulated images, as we need to know the exact position of the edges in advance. Let us first consider a "cartoon image" composed of vertical bands of increasing width, from 2 to 18 pixels. The ratio between the reflectivities of the bright and the dark lines is $12dB$. This reference image was multiplied with a simulated single-look speckle image. The correlation coefficients of the speckle is $\rho(1) = 0.42$, $\rho(2) = 0.03$, and $\rho(m) = 0$, $m > 2$, in azimuth as well as in range. The ideal image and its single-look speckled counterpart are shown in amplitude in Fig. 5 (a) and (b), respectively. Edge strength maps were calculated on the speckled image with both operators. Single-look images are extremely noisy, so strong smoothing is necessary. The ROEWA operator with $b = 0.9$ produced a very regular edge strength map giving rise to few false edges. To obtain the same reduction of speckle variance with a half window for both operators, and thus the same false alarm rate for a given detection threshold, the window size for the ROA operator was set to 39×39 (see the Appendix). A threshold of 1.85 gave the best compromise between the detection of real edges and the suppression of false ones.

The resulting segmentations are shown in Fig. 5 (c) and (d). The ROEWA operator gives a systematic detection of edges for bands of width 8 or higher, whereas the ROA operator detects systematically only from width 13. Some spurious edges are present near the edges in the case of the ROA operator. The experiment indicates that the ROEWA operator has better spatial resolution than the ROA oper-

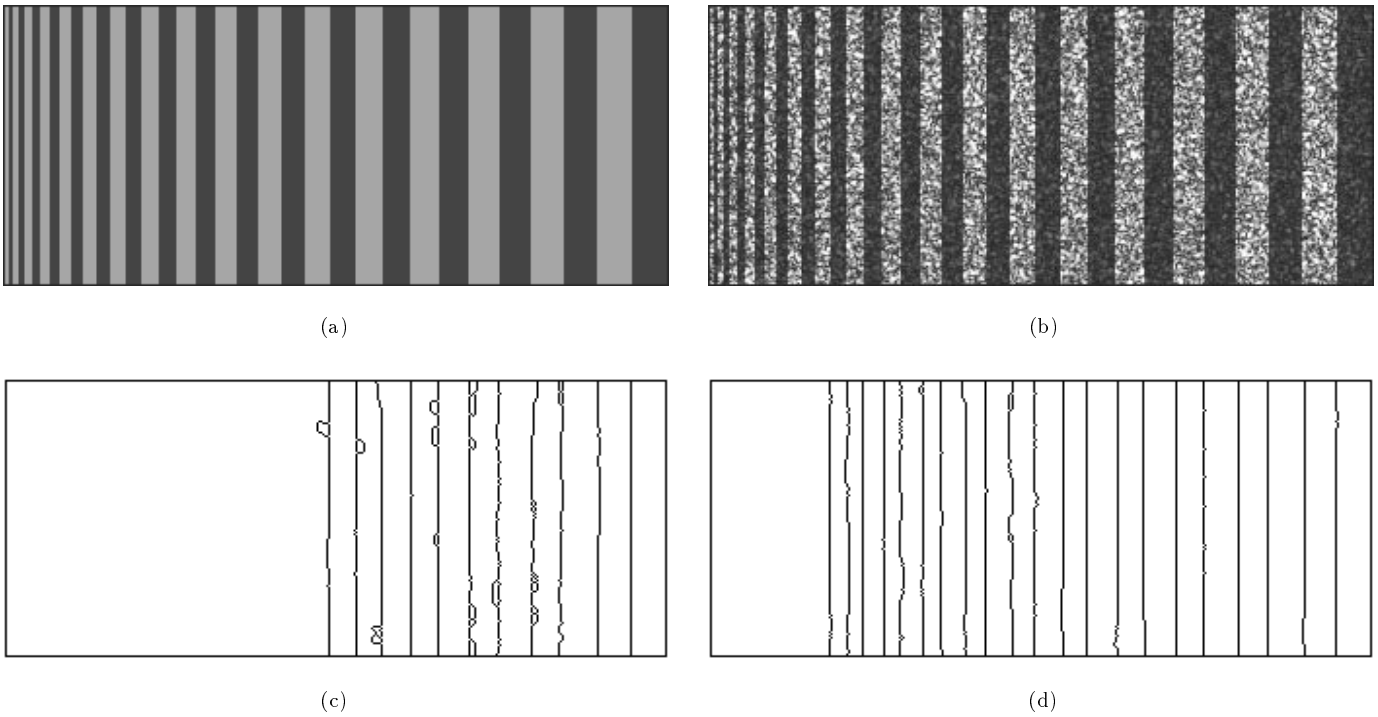

(a) (b) (c) (d)

Fig. 5. (a) Ideal image consisting of vertical lines of width 2 to 18 pixels. (b) The simulated single-look speckled image. (c) The segmentation obtained with the ROA edge detector and watershed thresholding. (d) The segmentation obtained with the ROEWA edge detector and watershed thresholding.

ator, for a given speckle reduction capacity. However, we have chosen a very strong smoothing to place ourselves in a multiedge situation. We could of course use a smaller window and detect edges at at finer scales with the ROA operator, at the risk of a higher false alarm rate.

Let us now examine a more realistic case. We synthesized the cartoon image shown in amplitude in Fig. 6 (a) by a first order Markov random field with four classes. The reflectivity ratio between subsequent classes is $6dB$. This image approximately corresponds to the multiedge model presented in section III-A. The mean region width $1/\lambda = 13.4$ pixels. Fig. 6 (b) shows the same image multiplied with single-look speckle. The correlation properties of the speckle are the same as in the previous example. To compare the performance of the edge detectors, we use Pratt's figure of merit [18]:

$$\mathcal{P} = \frac{1}{\max\{\mathcal{N}_{DE}, \mathcal{N}_{ID}\}} \sum_{i=1}^{\mathcal{N}_{DE}} \frac{1}{1+\beta d_i^2},$$

where $\mathcal{N}_{ID}$ is the number of ideal edge pixels, $\mathcal{N}_{DE}$ is the number of detected pixels and d_i is the distance between the ith detected edge pixel and the closest true edge pixel. β is a calibration constant that is usually set to one. However, as the edges are dense in our test image, so that the nearest ideal edge pixel never is far away, we set $\beta = 2$ for a stronger penalization of misplaced edge pixels. We accept the closest pixel on each side of a transition as an ideal edge pixel, i.e., $d_i = 0$ for every pixel having at least one pixel belonging to another region in its 4-neighborhood. The distance d_i to an ideal edge for the remaining pixels is obtained as follows: $d_i = 1$ is attributed to all remaining pixels having one or more pixels with $d_i = 0$ in their 4-neighborhood. Among the pixels not yet attributed, $d_i = 2$ is set for every pixel having at least one pixel with $d_i = 1$ in its 4-neighborhood, and so forth.

Edge strength maps were computed by the ROA operator with window sizes from 3×3 to 19×19 and by the ROEWA operator with the parameter b varying over the range 0.1 to 0.8. For each edge strength map the detection threshold maximizing Pratt's figure of merit was determined. Fig. 7 shows the result. The unit along the horizontal axis is the equivalent number of independent pixels in each half of the analyzing window in terms of the speckle reduction obtained by smoothing (see the Appendix). This allows us to compare the results obtained with the ROA operator with different window sizes, with those obtained by the ROEWA operator using exponential weighting functions of varying slope. From Fig. 7 we see that the ROEWA operator yields a better score than the ROA operator over most of the parameter range. However, the difference is relatively small near the maximum of the graphs, and for one window size (7×7) the ROA operator performs even better than the ROEWA operator. The difference in favor of the ROEWA operator increases with stronger smoothing. This reflects the fact that the multiedge model is more relevant the larger the analyzing window is. The ROA operator is optimal in the monoedge case, which is more frequently encountered when using small windows. The localization of the maxima of the graphs should not be taken too literally. Such a weak smoothing generally implies an important number of false edges due to speckle. A stronger smoothing gives more meaningful boundaries. The theoretical optimum for the ROEWA operator, according to (7), is $b = 0.74$, which corresponds to about 30 independent pixels in each half window.

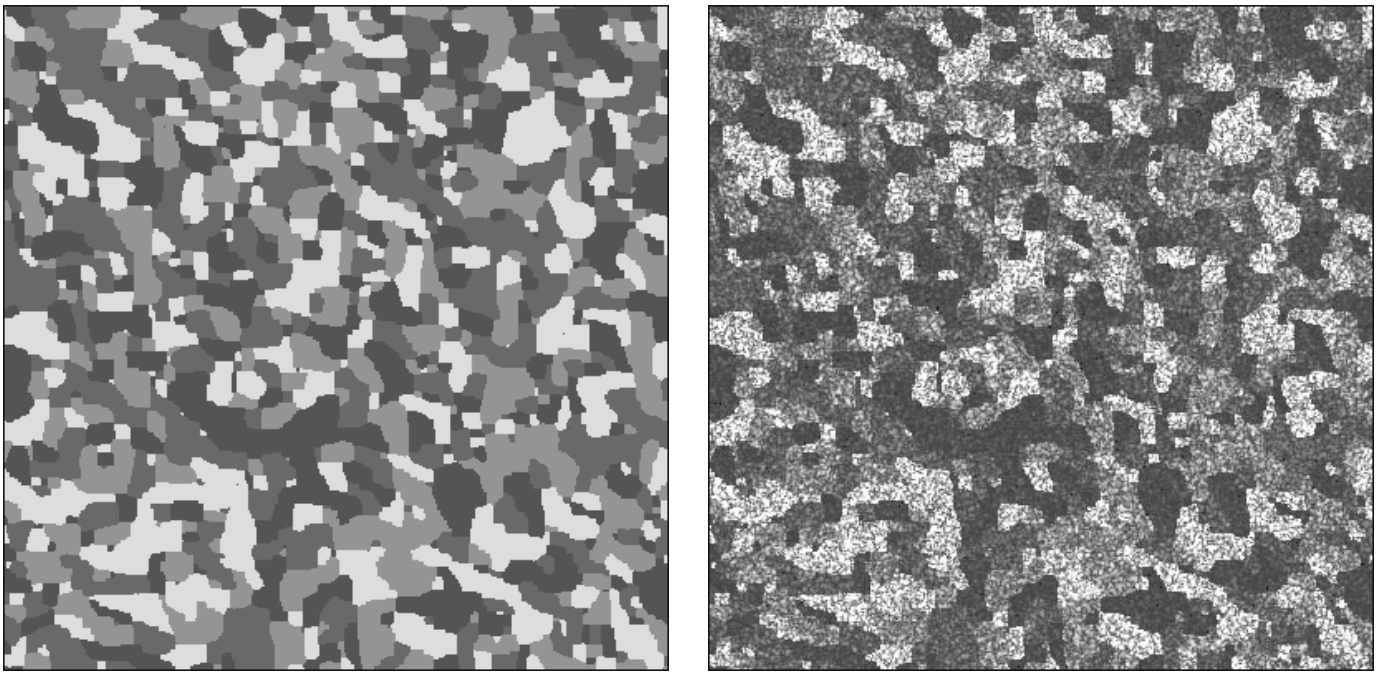

(a) (b)

Fig. 6. (a) Ideal image synthesized by a first order Markov random field. (b) The corresponding single-look speckled image.

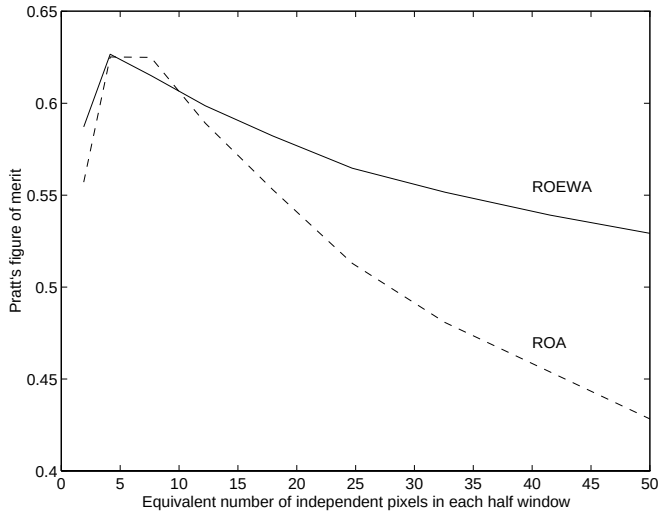

Fig. 7. Pratt's figure of merit for the ROA edge detector with varying window size, and for the ROEWA edge detector with varying slope, applied to the single-look speckled Markov random field image.

Results on real world data are a useful supplement to simulations, but here only a visual appreciation can be given. A multitemporal series of three-look ERS-1 images of an agricultural scene near Bourges, France, was used to test edge detectors and post-processing. An extract of a color composition of 3 dates acquired with monthly intervals is shown in Fig. 8. Note the close resemblance between this scene and the simulated image in Fig. 6. The edge strength maps of the different dates were averaged, supposing that no geometrical changes took place between the acquisitions and that the images are perfectly registered. Our strategy is to allow a strong over-segmentation in the edge detection step, and then rely on subsequent merging to eliminate false edges. The best results were obtained with a 13×13 window for the ROA operator and with $b = 0.73$ for the ROEWA operator. Given the speckle correlation, the two detectors have about the same speckle reduction capacity with these parameters. Visual inspection of the segmentations revealed only slight differences in favor of the ROEWA operator. We shall use this image to illustrate how complementary post-processing can improve the final result. Fig. 9 shows the initial segmentation, obtained with the ROEWA operator with parameter $b = 0.73$ and the modified watershed algorithm with threshold 1.53. The threshold was deliberately set very low to make sure that practically all significant edges are detected, resulting in a massively over-segmented image. All the three merging criteria mentioned in section III-E were compared. The LR measure (13) gave the result which agreed best with our conception of the regions. The unequal variance Student's t-test gave similar results, whereas the classic Student's t-test performed poorly. In the final segmentation shown in Fig. 10, the number of regions has been reduced from over 5000 to about 600. Adjacent regions for which the log-likelihood $\ell_{\text{merge}} > -1.85$ for all three dates were merged. The threshold indicates that we accepted some irregularities within the regions. In addition, regions containing only one pixel were supposed to be due to speckle and thus eliminated. The merging order was defined by the iterative pairwise mutually best merge criterion. Almost all regions that we can distinguish by eye have been detected. Some regions still seem to be split in several parts, the edges are sometimes irregular due to speckle, and the corners are slightly rounded due to the strong smoothing used by the edge detector. It is, nevertheless, a surprisingly good SAR image segmentation.

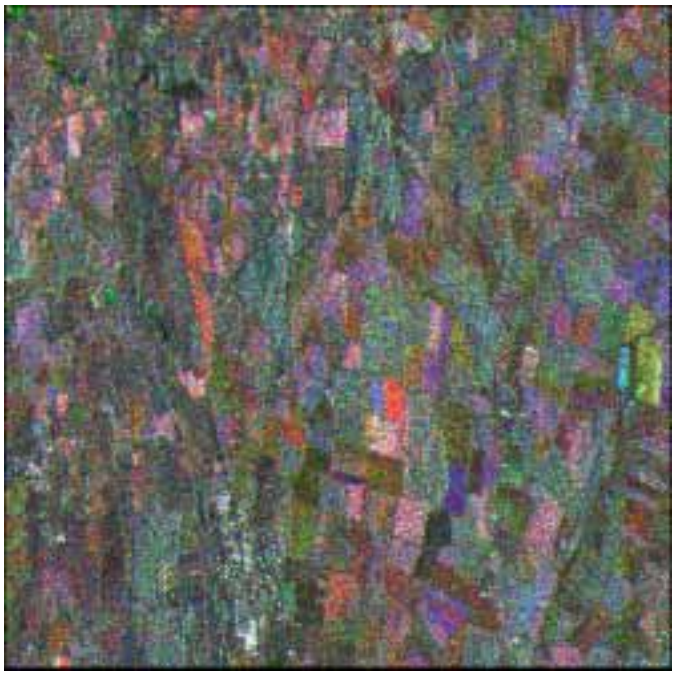

Fig. 8. Extract of a color composition of three SAR images of an agricultural scene near Bourges, France ©ESA – ERS-1 data – 1993, Distribution SPOT Image.

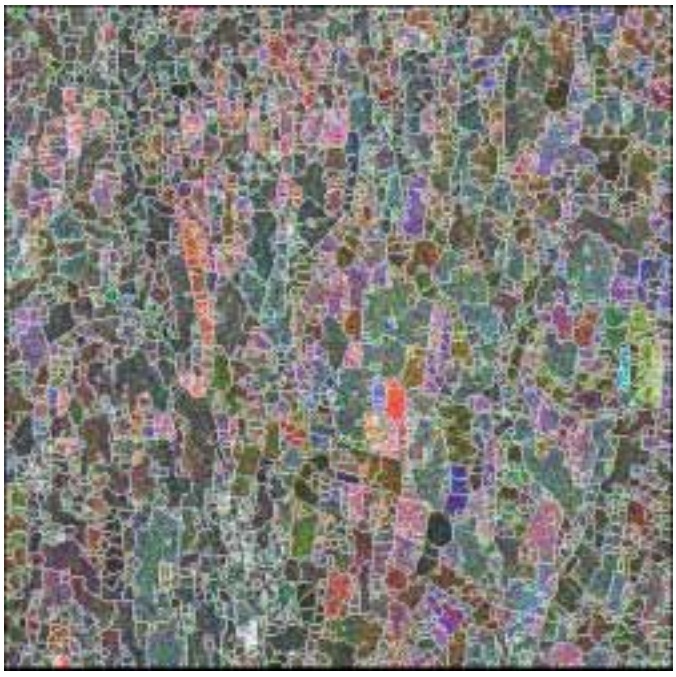

Fig. 9. Over-segmented image obtained by the ROEWA operator and watershed thresholding.

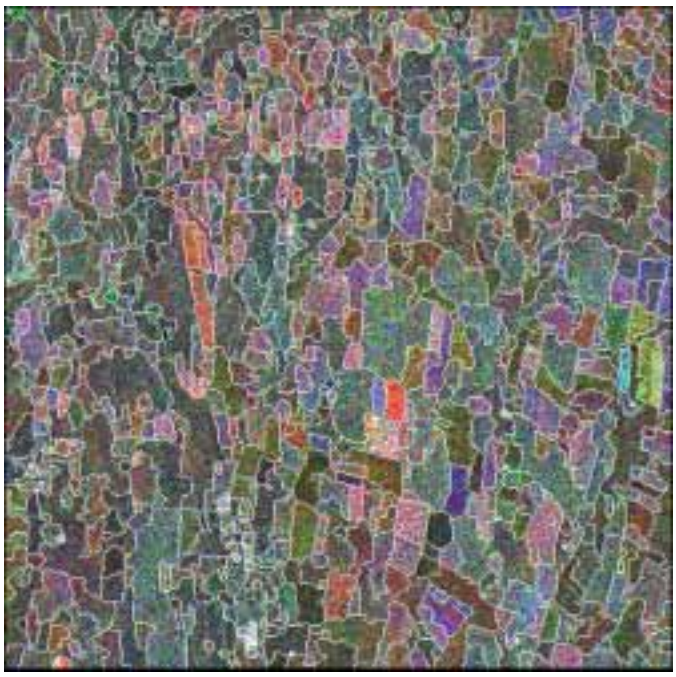

Fig. 10. Segmentation obtained by the ROEWA operator, watershed thresholding and region merging.

V. Discussion

The estimator of local means used by the ROEWA operator is optimized for a stochastic multiedge model. We have shown that an exponentially weighted mean with a correctly adjusted slope gives the optimal tradeoff between localization precision and speckle suppression when the reflectivity jumps follow a Poisson distribution. This multiedge model is primarily adapted to describe scenes composed of distinct regions of relatively uniform reflectivity, but of strongly varying size. Exponential weighting is strictly optimal only for scene types which correspond exactly to the stochastic image model. Moreover, we supposed uncorrelated speckle. Equivalent estimators for other scene models and for correlated speckle can be developed by substituting the appropriate spectral density functions into (6), but the impulse response will in general not be any simple, analytic function like the one that we found here.

The arithmetic mean, used by the ROA operator, is the ML estimator of the mean value for a stationary process. The ROA operator is hence spatially optimal in a monoedge context, i.e., when the distance between edges is larger than the width of a half window. If the regions generally are big, as compared to the window size that is necessary to obtain a sufficient speckle suppression, the ROA operator is bound to perform better than the ROEWA operator.

To decide whether or not the ROEWA operator can bring an improvement, as compared to the ROA operator for a given image, several factors must be considered: the average region size and the variations in region size, the contrast between different regions, the ENIL, and the speckle correlation. The ROEWA should theoretically perform better than the ROA operator when the reflectivity approximately corresponds to the multiedge model, the mean region width is small, and the ENIL is low. With increasing ENIL or mean region width, the monoedge model becomes more appropriate, and the ROA operator can be expected to perform better.

The experimental results confirm the theoretical discussion above. Edge detection on a single-look image composed of vertical bands of gradually increasing width indicate that the ROEWA detector permits a strong speckle reduction without degrading the spatial resolution as much

as the ROA operator. Here we have deliberately placed ourselves in a rather extreme multiedge situation.

On another simulated single-look image, where the reflectivity closely approximates the proposed multiedge model, the ROA and ROEWA detectors were compared over a wide range of window sizes and corresponding slopes of the exponential weighting function, in terms of Pratt's figure of merit. For the smallest windows, the monoedge hypothesis is generally verified and the superiority of the ROA operator is confirmed, even though the scores are very close. With stronger smoothing, corresponding to larger windows, the multiedge model becomes more relevant, and the performance difference in favor of the ROEWA operator increases steadily. Strong smoothing is here necessary to avoid numerous false edges due to speckle, due to the low ENIL and the high speckle correlation.

A hybrid segmentation scheme, which combines the proposed edge detection method with LR region merging, was shown to give excellent results on multitemporal ERS-1 images of an agricultural scene. The difference between the results obtained by the ROA and ROEWA operators was small. This reflects the fact that typical regions are so large that the monoedge model is just as appropriate as the multiedge model for the window size used. Such segmentations can e.g., be used to improve thematic classifications [19]. It should be stressed that this is a very rapid segmentation method. On a Silicon Graphics INDY workstation with a MIPS R4400 200MHz CPU and 64 MB of memory, the ROEWA operator, the watershed thresholding, and the LR region merging needed only 12 s to process three channels of 512×512 pixels to produce the result in Fig. 10. This makes our method more than an order of magnitude faster than another sophisticated SAR segmentation scheme, the RWSEG algorithm [5], which is implemented in the CAESAR module of the ERDAS IMAGINE software package. The quality of the results are comparable.

VI. Conclusion

In this article, we propose a new CFAR edge detector for SAR images, which is optimal under a stochastic multiedge model. It has been shown to perform better than the ROA operator for images which closely approximate the multiedge model, especially when the average region width is small and the ENIL is low. The ROEWA operator, watershed thresholding, and LR region merging constitute a very efficient segmentation scheme. The watershed thresholding can be replaced by more advanced edge extraction methods, e.g., based on the powerful concepts of basin dynamics [20] and edge dynamics [21].

The ROEWA operator is a simple, nonadaptive edge detector. There are several other approaches to edge detection and segmentation in a multiedge context. Multiresolution ROA operators [22] combine the ratios computed with different window sizes according to their statistical significance. The ideal solution would be a spatially adaptive LR operator, which varies the window size, the window form and the way it is split, so that the local arithmetic means are estimated on complete, uniform regions. However, these perfectly homogeneous zones are unknown, and difficult to identify in the presence of speckle. The practical solution is to try to iterate towards the best segmentation. The RWSEG algorithm [5], for example, combines edge detection and region growing iteratively. Stochastic methods based on Markov random fields and simulated annealing [8] iterate towards a segmentation which minimizes a global cost function. Such methods may give even better results, at the cost of a higher computational complexity.

Appendix

Let us suppose the intensity I to be a wide-sense stationary process. Taking the block-average of N pixels, $\hat{\mu}_{Ib} = 1/N \sum_{k=1}^{N} I_k$, reduces the variance with a factor N if the pixels are uncorrelated

$$\sigma^2_{Ibu} = \frac{\sigma^2_I}{N}$$

If the pixels are correlated

$$\sigma^2_{Ibc} = \frac{\sigma^2_I}{N^2} \sum_{k=1}^{N} \sum_{l=1}^{N} \rho(|k-l|) \tag{14}$$

where $\rho(m)$, $m \geq 0$, are the autocorrelation coefficients.

In SAR images, the speckle correlation typically becomes insignificant for distances superior to 2 or 3 pixels. More generally, we may suppose $\rho(m) = 0, m > M$, and $M \ll N$, so that (14) can be rewritten as

$$\sigma^2_{Ibc} = \frac{\sigma^2_I}{N^2} \left[N + 2 \sum_{k=1}^{M} (N-k)\rho(k) \right]. \tag{15}$$

The factor with which the variance is reduced gives us the equivalent number of independent pixels in the analyzing window. Let us now consider the speckle reduction obtained by one half window of the ROEWA operator. We first employ the ISEF f in one direction

$$\begin{aligned}
\sigma^2_{Ifc} &= \sigma^2_I \sum_{k=-\infty}^{\infty} \sum_{l=-\infty}^{\infty} f(k) f(l) \rho(k-l) \\
&= \sigma^2_I \left(\frac{1-b}{1+b} \right)^2 \sum_{k=-\infty}^{\infty} \sum_{m=-M}^{M} b^{|k|+|k+m|} \rho(m) \\
&= \sigma^2_I \left(\frac{1-b}{1+b} \right)^2 \sum_{m=-M}^{M} \left[|m| + \frac{1+b^2}{1-b^2} \right] b^{|m|} \rho(|m|).
\end{aligned}$$

The normalized causal filter f_1 in the perpendicular direction gives

$$\begin{aligned}
\sigma^2_{If_1c} &= \sigma^2_{Ifc} \sum_{k=0}^{\infty} \sum_{l=0}^{\infty} f_1(k) f_1(l) \rho(k-l) \\
&= \sigma^2_{Ifc} \frac{(1-b)^2}{1-b^2} \left[1 + 2 \sum_{m=1}^{M} b^{3m} \rho(m) \right].
\end{aligned}$$

The equivalent number of independent pixels in a half window of the ROEWA operator is thus $\sigma^2_I / \sigma^2_{If_1c}$, which can be compared to the corresponding number for a half window of the ROA operator obtained by employing (15) in the horizontal and vertical direction.

Acknowledgments

The authors acknowledge the valuable contributions of F. Lebon, N. Mauduit, F. Séry, J. Cabada, C. Lemarechal, C. Fortier, and T. Rabaute.

References

[1] R. Touzi, A. Lopès, and P. Bousquet, "A statistical and geometrical edge detector for SAR images," *IEEE Trans. Geosci. Remote Sensing*, vol. GE-26, pp. 764-773, Nov. 1988.

[2] A. C. Bovik, "On detecting edges in speckle imagery," *IEEE Trans. Acoust. Speech Signal Processing*, vol. ASSP-36, pp. 1618-1627, Oct. 1988.

[3] V. S. Frost, K. S. Shanmugan, and J. C. Holtzman, "Edge detection for synthetic aperture radar and other noisy images," in *Proc. IGARSS*, Munich, Germany, June 1982, sec. FA2, pp. 4.1-4.9.

[4] C. J. Oliver, D. Blacknell, and R. G. White, "Optimum edge detection in SAR," *Inst. Elec. Eng. Proc. Radar Sonar Navigat.*, vol. 143, Feb. 1996.

[5] R. G. White, "Change detection in SAR imagery," *Int. J. Remote Sensing*, vol. 12, no. 2, pp. 339-360, 1991.

[6] R. Cook and I. McConnell, "MUM (Merge Using Moments) segmentation for SAR images," in *Proc. EurOpto SAR Data Processing for Remote Sensing*, Rome, Italy, 1994, vol. SPIE 2316, pp. 92-103.

[7] D. M. Smith, "Speckle reduction and segmentation of Synthetic Aperture Radar images," *Int. J. Remote Sensing*, vol. 17, no. 11, pp. 2043-2057, 1996.

[8] R. Cook, I. McConnell, D. Stewart, and C. J. Oliver, "Segmentation and simulated annealing," in *Proc. EurOpto SAR Image Analysis and Modelling II*, Taormina, Italy, Sept. 1996, vol. SPIE 2958, pp. 30-37.

[9] F. T. Ulaby, R. K. Moore, and A. K. Fung, *Microwave Remote Sensing*, vol. 3, Dedham, MA: Artech House, 1986.

[10] J. Stern, J. de Barbeyrac, and R. Poggi, *Méthodes Pratiques d'Etude des Fonctions Aléatoires*, Paris, France: Dunod, 1967.

[11] V. S. Frost, K. S. Shanmugan, and J. C. Holtzman, "A model for radar images and its application to adaptive filtering of multiplicative noise," *IEEE Trans. Pattern Anal. Mach. Intell.*, vol. 4, pp. 165-177, Mar. 1982.

[12] J. W. Woods and J. Biemond, "Comments on "A model for radar images and its application to adaptive filtering of multiplicative noise"," *IEEE Trans. Pattern Anal. Mach. Intell.*, vol. 6, pp. 658-659, Sept. 1984.

[13] J. Shen and S. Castan, "An optimal linear operator for step edge detection," *CVGIP: Graph. Models Image Processing*, vol. 54, pp. 112-133, Mar. 1992.

[14] R. Fjørtoft, P. Marthon, A. Lopès, and E. Cubero-Castan, "Edge detection in radar images using recursive filters," *Proc. ACCV*, Singapore, Dec. 1995, vol. 3, pp. 87-91.

[15] L. Vincent and P. Soille, "Watersheds in digital spaces: An efficient algorithm based on immersion simulations," *IEEE Trans. Pattern Anal. Mach. Intell.*, vol. 13, pp. 583-598, May 1991.

[16] P. Marthon, B. Paci, and E. Cubero-Castan, "Finding the structure of a satellite image," in *Proc. EurOpto Image and Signal Processing for Remote Sensing*, Rome, Italy, 1994, vol. SPIE 2315, pp. 669-679.

[17] A. Baraldi and F. Parmiggiani, "Segmentation driven by an iterative pairwise mutually best merge criterion," in *Proc. IGARSS*, Firenze, Italy, July 1995, pp. 89-92.

[18] W. K. Pratt, *Digital Image Processing*, New York: Wiley, 1978.

[19] Franck Sery, A. Lopès, D. Ducrot-Gambart, R. Fjørtoft, E. Cubero-Castan, and P. Marthon, "Multisource classification of SAR images with the use of segmentation, polarimetry, texture and multitemporal data," in *Proc. EurOpto Image and Signal Processing for Remote Sensing*, Taormina, Italy, Sept. 1996, vol. SPIE 2955, pp. 186-197.

[20] M. Grimaud, "A new mesure of contrast: Dynamics," in *Proc. Image Algebra and Morphological Processing*, San Diego, July 1992, vol. SPIE 1769, pp. 292-305.

[21] L. Najman and M. Schmitt, "Geodesic saliency of watershed contours and hierarchical segmentation," *IEEE Trans. Pattern Anal. Mach. Intell.*, vol. 18, pp. 1163-1173, Dec. 1996.

[22] R. Fjørtoft, A. Lopès, P. Marthon, and E. Cubero-Castan, "Different approaches to multiedge detection in SAR images," *Proc. IGARSS*, Singapore, Aug. 1997.

Roger Fjørtoft received the M.Sc. degree from the Department of Telecommunications, Norwegian Institute of Technology (NTH), Trondheim, Norway, in 1993. Since 1995 he is pursuing the Ph.D. degree at the Ecole Nationale Supérieure d'Electrotechnique, d'Electronique, d'Informatique et d'Hydraulique de Toulouse (ENSEEIHT), Toulouse, France, and at the Centre d'Etudes Spatiales de la Biosphère (CESBIO), Toulouse, France. His main research interests are in segmentation and multiresolution analysis of SAR images.

Armand Lopès received the engineering degree from the Ecole Nationale Supérieure de l'Aéronautique et de l'Espace (Sup'Aéro), Toulouse, France, and the Ph.D. degree from the Université Paul Sabatier (UPS), Toulouse, France, in 1983. He is now Maître de Conférences at UPS, teaching physics. At the Centre d'Etude Spatiale des Rayonnements (CESR) he studied the microwave extinction and scattering by vegetation, the SAR and scatterometer image processing. Since 1995 he is at the Centre d'Etudes Spatiales de la Biosphère (CESBIO), where his main activities concern SAR image post-processing.

Philippe Marthon received the engineering degree and the Ph.D. in computer science from the Ecole Nationale Supérieure d'Electrotechnique, d'Electronique, d'Informatique et d'Hydraulique de Toulouse (ENSEEIHT), Toulouse, France, in 1975 and 1978, respectively, and the Doctorat d'Etat degree from the Institut National Polytechnique de Toulouse (INPT), in 1987. He is currently Maître de Conférences at ENSEEIHT and research scientist at the Institut de Recherche en Informatique de Toulouse (IRIT). His research interests include image processing and computer vision.

Eliane Cubero-Castan received the Ph.D. in computer science, software engineering from the Université Paul Sabatier (UPS), Toulouse, France, in 1984. She is now with the French Space Agency (CNES), in the Space Image Quality and Processing Division, where she has the onus of research and development project management in the field of information extraction (classification, segmentation, and network and urban area extraction) from optical, radar and multisensor remote sensing data.